# Vibrational properties of noble gas endohedral fullerenes

**ARTICLE** *in* PHYSICAL CHEMISTRY CHEMICAL PHYSICS · MAY 2011

Impact Factor: 4.49 · DOI: 10.1039/c1cp20279k · Source: PubMed



**5 AUTHORS**, INCLUDING:

Cimpoesu Fanica
Institute of Physical Chemistry
**77** PUBLICATIONS **872** CITATIONS
SEE PROFILE

Seitaro Ito
Tohoku University
**32** PUBLICATIONS **240** CITATIONS
SEE PROFILE

Nita Dragoe
Université Paris-Sud 11
**132** PUBLICATIONS **1,197** CITATIONS
SEE PROFILE

PCCP

Dynamic Article Links

Cite this: *Phys. Chem. Chem. Phys.*, 2011, **13**, 9609–9615

www.rsc.org/pccp

**PAPER**

# Vibrational properties of noble gas endohedral fullerenes†

**Fanica Cimpoesu,*[a] Seitaro Ito,[b] Hidekazu Shimotani,[c] Hidenori Takagi[bd] and Nita Dragoe*[e]**

***Received 1st February 2011, Accepted 15th March 2011***
**DOI: 10.1039/c1cp20279k**

Analysis of IR and Raman spectra of $Ar@C_{60}$ and $Kr@C_{60}$ shows that the incorporation of noble gas atoms causes a blue shift of low energy vibrations, which have radial character, and a red shift of higher energy ones which have a tangential character movement. The mechanism of these phenomena is explained on the basis of *ab initio* numerical experiments with DFT and MP2 procedures. Methodological discussions are advanced, altogether with a scheme for the estimation of the van der Waals interaction between fullerene and noble gas, based on the frequency shifts.

## Introduction

One interesting feature of small cage fullerenes is the ability to incorporate and stabilize atoms[1] or small molecules.[2] Noble gas-containing endohedral fullerenes are well known,[3] but several fundamental questions, such as the nature of the host–guest interactions, remain to be clarified.[4] In contrast to metal fullerene endohedrals,[5] since noble gas atoms are inert, little or no charge transfer takes place between the encapsulant and the cage and the $I_h$ symmetry is conserved. This is consistent with the NMR spectroscopy data of He,[6] Kr[7] and Xe[8] samples, EXAFS[9] and X-ray crystal structure analysis[10] of $Kr@C_{60}$, recently X-ray photoelectron spectroscopy[11] of $Ar@C_{60}$ and most of the theoretical calculations.[12] Noble gas endohedral fullerenes are traditionally synthesized by high pressure/high temperature techniques using KCN as a catalyst as originally proposed by Cross *et al.*[13] The major challenge with this process is the chromatographic purification of reaction products, a difficulty that originates from structural similarities between $A@C_{60}$ and $C_{60}$. With extensive purification, both $Kr@C_{60}$ and $Ar@C_{60}$[17] were isolated, and $Xe@C_{60}$ was enriched. The availability of high purity endohedral material enabled detailed studies of their physical properties. Vibrational spectroscopy is particularly useful because it is a sensitive local probe of subtle cage modifications that originate from encapsulation. For instance, infrared (IR) spectroscopy results are consistent with negative thermal expansion for $Kr@C_{60}$.[14]

In order to investigate the detailed perturbations to cage vibrations in endohedral fullerenes; we carried out a joint experimental and theoretical study of $Ar@C_{60}$ and $Kr@C_{60}$. Following the concept of $C_{60}$ aromaticity revealed by $^3$He-NMR in $He@C_{60}$,[15] we point out that the encapsulant acts as a perturbation to cage vibrations. The external resemblance of the endohedral compounds to that of pristine $C_{60}$ (high symmetry is important for the mechanism of superconductivity in doped $C_{60}$)[16] supports the hypothesis that the endohedral fullerenes might become superconducting under appropriate doping conditions but have different characteristics: higher molecular mass, different vibration spectra, *etc*. Indeed, our recent work demonstrated that $K_3Ar@C_{60}$ and $Rb_3Ar@C_{60}$ display superconductivity at 17.8 and 26.8 K, respectively, significantly lower than that of pristine $C_{60}$.[17] Understanding the vibrational or electronic origin of this effect motivates our present investigation of these nanocarbon materials. We observed systematic frequency shifts which correlate directly with encapsulant size, aromatic character, and encapsulant–cage potential. Our work thus illuminates new aspects of the vibration chemistry of fullerenes, constructing new prerequisites for further advances in the superconductivity mechanisms, where the electron–phonon interactions involving $H_g$ modes are of acknowledged importance.[18]

## Experimental methods

$Ar@C_{60}$ and $Kr@C_{60}$ were prepared by a method similar to the one reported by Cross *et al.*[13] $C_{60}$ and KCN (**Warning**: poisonous material, to be carefully handled and disposed) were mixed at a weight ratio of 3 : 1 and ground in a mortar for about 20 min. The mixture was put into a copper tube that was previously pressed and arc welded at one end. The air in

[a] *Institute of Physical Chemistry, Splaiul Independentei 202, Bucharest 060021, Romania. E-mail: cfanica@yahoo.com; Fax: +40 21-3121147*
[b] *Department of Advanced Materials, University of Tokyo, Kashiwa-no-ha 5-1-5, Kashiwa 277-8561, Japan*
[c] *Quantum-Phase Electronics Center, School of Engineering, The University of Tokyo, 7-3-1, Hongo, Bunkyo-ku, Tokyo 113-8656, Japan*
[d] *RIKEN Advanced Science Institute, Hirosawa 2-1, Wako 351-0198, Japan*
[e] *Université Paris Sud XI, ICMMO, UMR 8182 CNRS, 91405 Orsay, France. E-mail: nita.dragoe@u-psud.fr*

† Electronic supplementary information (ESI) available: IR and Raman spectra for $Kr@C_{60}$, $Ar@C_{60}$ and $C_{60}$. A selective analysis of Hg vibration modes is given by using spherical harmonics. See DOI: 10.1039/c1cp20279k

the tube was pumped out and Kr gas at a pressure of 3 bar was inserted; the open end was then sealed by crimping. The tube was heated to 650 °C and 4000 atm by using hot isostatic pressing equipment (HIP) in which argon gas was used as the pressure medium. The product contained mostly $C_{60}$ and small amounts of Kr@$C_{60}$, and other impurities, such as Ar@$C_{60}$ when the copper tube was not perfectly sealed as well as other residual insoluble compounds, presumably polymeric fullerenes. To obtain Ar@$C_{60}$, a mixture of KCN and $C_{60}$ was placed directly in an alumina crucible in a HIP equipment with argon gas as the pressure medium. The mixture was then dissolved in toluene and the soluble part extracted, the solid containing KCN was discarded. The yield was ranging from 0.01% to 0.1% for both endohedrals.

The separation of Ar@$C_{60}$ and Kr@$C_{60}$ from the major $C_{60}$ phase was accomplished by using recycling HPLC. The column was a specially made preparative Cosmosil Buckyprep column (28 × 250 mm) and the flow rate was 50 ml $min^{-1}$ of toluene with injection volumes of 24 ml. After recycling five times, the latter half of the $C_{60}$ peak including Ar@$C_{60}$ and Kr@$C_{60}$ was collected. This operation was repeated four times. After the fourth separation, a similar four-stage separation was done using a preparative Buckyprep (20 × 250 mm) column with a flow rate of 20 ml $min^{-1}$ and injection volumes of 5 ml.[19] This procedure was applied for the separation of other endohedrals in our group.[20]

After the total of eight steps, about 0.5 mg of 99% Ar@$C_{60}$ and 0.15 mg of 99% Kr@$C_{60}$ were obtained. These steps were repeated several times and mg scale pure Ar@$C_{60}$ were obtained. FT-Raman spectra were measured at 1 $cm^{-1}$ resolution on JEOL RS-RSU200 using a Nd:YAG laser (1064 nm). The laser intensity was 100 mW. The samples (about 0.1 mg) were dissolved in *o*-dichlorobenzene and deposited onto a glass substrate. The solvent was removed under dynamic vacuum at room temperature for 1 day. To increase the detected dispersion light, the bottom of glass was covered with a gold foil as a reflector of the laser and dispersion light penetrating a sample.

FT-IR spectra were obtained on JEOL JIR-6500 with a microscope unit (IR-MAU110) at a resolution of 0.5 $cm^{-1}$ in the transmission mode. The samples were dissolved in 10 ml of *o*-dichlorobenzene and deposited onto KBr windows. The solvent was removed under dynamic vacuum at room temperature for 1 day. The sample compartment was purged by dry air.

All calculations were carried out using Gaussian98 program.[21] Making use of Hartree–Fock (HF), Density Functional Theory (DFT with B3LYP functional) and MP2 methods we chose the 6-31G* basis set as the best compromise for all of them, since richer bases are too demanding in the MP2 step.

## Results and discussion

### Vibration shifts in $A$@$C_{60}$ *vs.* $C_{60}$ ($A$ = Ar, Kr)

From group theory, 46 vibration modes are expected for the $C_{60}$ molecule (with various degeneracies in the $I_h$ symmetry). Two $A_g$ and eight $H_g$ modes are Raman active.[22] In the Raman spectra of $C_{60}$, Ar@$C_{60}$ and Kr@$C_{60}$ (see ESI†) only eight bands were clearly observed. Two weak $H_g$ bands were not considered; these two are observed in the spectra but have a small signal/noise ratio. This is probably due to the small amount of sample used and the long wavelength laser used for excitation. Along the series, the relative intensities are similar. The IR spectra (see ESI†) for the three compounds measured in the same conditions consist of four bands corresponding to the $T_{1u}$ modes in the $I_h$ symmetry, a classical characteristic of the icosahedral fullerene. In the spectrum of Ar@$C_{60}$, some additional bands, whose intensity became smaller as HPLC separation was repeated, were assigned to impurities. Their presence does not impinge upon the present analysis.

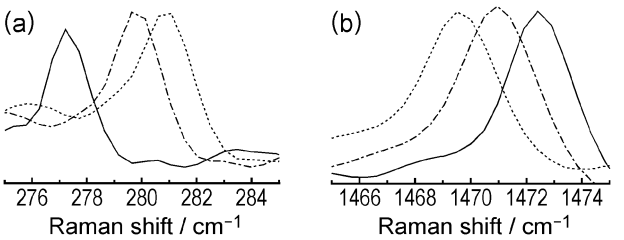


**Fig. 1** Details of Raman spectra of $C_{60}$ (—), Ar@$C_{60}$ (-·-) and Kr@$C_{60}$ (···) around (a) 280 $cm^{-1}$ and (b) 1470 $cm^{-1}$.

The IR and Raman bands of Ar@$C_{60}$ and Kr@$C_{60}$ show small but systematic shifts, as compared to the pristine $C_{60}$. A detail is shown in Fig. 1. The encapsulated noble gas atom caused the blue shift of Raman frequencies lower than about 510 $cm^{-1}$ and the red shift of those higher than about 770 $cm^{-1}$. The shifts were 0.5–2.4 $cm^{-1}$ in Ar@$C_{60}$ and 0.5–5.3 $cm^{-1}$ in Kr@$C_{60}$. Each wavenumber shift of Kr@$C_{60}$ was larger than or equal to that of Ar@$C_{60}$. Table 1 lists IR and Raman frequencies for $C_{60}$ and the shifts for $A$@$C_{60}$, and their band widths.

The IR bands were shifted in a manner similar to Raman spectra. The encapsulated noble gas atom causes the blue shift of the lower two vibration modes (around 528 $cm^{-1}$ and 575 $cm^{-1}$), and the red shift of the two higher ones (around 1182 $cm^{-1}$ and 1428 $cm^{-1}$), except for the vibration of Kr@$C_{60}$ around 575 $cm^{-1}$. The shifts were 0.5–2.0 $cm^{-1}$ in Ar@$C_{60}$ and 0–2.0 $cm^{-1}$ in Kr@$C_{60}$. The Raman bands were slightly broadened by encapsulation of Ar and Kr atoms. In contrast, the IR bands became narrower than the pristine $C_{60}$.

### *Ab initio* calculations and methodology

The observed vibration effects were rationalized with the help of *ab initio* calculations and analytical models. The particular situation of *van der Waals* interaction in highly symmetrical environment offers opportunities for methodological discussion. The experimental shift tendencies, toward blue in lower frequencies and to red in the higher ones, are reproduced qualitatively well at the HF level. In spite of the poor absolute match of HF vibration numbers to the experiment, the computed relative shifts are paralleling the tendencies in higher *vs.* lower modes (see Table 1).

The DFT calculations show sensitively improved accordance to the experiment for the absolute values of computed frequencies. A uniform scaling by 0.98 of the B3LYP/6-31G*

 

**Table 1** Experimental and computed vibration data. Frequencies for the $C_{60}$ reference ($\omega$) and shifts ($\Delta\omega$) corresponding to the encapsulate systems. The experimental data are completed with the recorded bandwidth. The $A_g$ and $H_g$ rows correspond to Raman and the $T_{1u}$ rows to infrared spectra. $\sigma$ is the bandwidth (half-maximum full-width). All quantities are in $cm^{-1}$

| | Experimental | | | | | | HF/6-31G* | | | B3LYP/6-31G* | | |
|---|---|---|---|---|---|---|---|---|---|---|---|---|
| | $C_{60}$ | $Ar@C_{60}$ | $Kr@C_{60}$ | $C_{60}$ | $Ar@C_{60}$ | $Kr@C_{60}$ | $C_{60}$ | $Ar@C_{60}$ | $Kr@C_{60}$ | $C_{60}$ | $Ar@C_{60}$ | $Kr@C_{60}$ |
| | $\omega$ | $\Delta\omega$ | $\Delta\omega$ | $\sigma$ | $\sigma$ | $\sigma$ | $\omega$ | $\Delta\omega$ | $\Delta\omega$ | $\omega$ | $\Delta\omega$ | $\Delta\omega$ |
| $A_g$ | 500.9 | 0.5 | 0.5 | 1.5 | 2.4 | 2.9 | 526.7 | 0.3 | 0.9 | 497.0 | −0.9 | −1.8 |
| $A_g$ | 1472.4 | −1.4 | −2.9 | 3.4 | 3.4 | 3.4 | 1600.4 | −3.1 | −4.1 | 1502.7 | −2.7 | −3.4 |
| $H_g$ | 277.2 | 2.4 | 3.9 | 2 | 1.9 | 2.4 | 289.1 | 3.5 | 5.9 | 266.9 | 3.3 | 2.8 |
| $H_g$ | 436.8 | 2.4 | 5.3 | 6.8 | 11.1 | 8.7 | 482.3 | 5.5 | 7.2 | 437.7 | 4.3 | 2.7 |
| $H_g$ | 709.0 | | | | | | 794.4 | 1.8 | −1.9 | 719.2 | 2.6 | −5.0 |
| $H_g$ | 777.2 | −0.5 | −1.0 | 3.4 | 4.3 | 4.3 | 840.5 | −1.3 | −1.6 | 787.9 | −1.8 | −2.6 |
| $H_g$ | 1105.0 | −0.9 | −3.3 | 5.3 | 7.7 | 6.8 | 1208.2 | −2.1 | −2.7 | 1127.6 | −1.7 | −2.3 |
| $H_g$ | 1255.5 | −3.9 | −5.4 | 9.2 | 9.6 | 7.7 | 1379.9 | −2.8 | −3.4 | 1276.4 | −1.8 | −2.6 |
| $H_g$ | 1425.0 | | | | | | 1561.7 | −2.5 | −3.3 | 1454.8 | −2.7 | −2.8 |
| $H_g$ | 1578.5 | −1.5 | −2.9 | 8.2 | 10.1 | 10.6 | 1791.4 | −2.1 | −3 | 1617.5 | −2.2 | −2.8 |
| $T_{1u}$ | 526.2 | 2.0 | 2.0 | 5.5 | 3.4 | 3.9 | 598.6 | 2.0 | 0.1 | 537.1 | 4.2 | 1.9 |
| $T_{1u}$ | 575.9 | 1.0 | 0.0 | 3.6 | 2.7 | 1.9 | 624.8 | −0.5 | −0.1 | 590.2 | 0.1 | 4.5 |
| $T_{1u}$ | 1182.7 | −0.5 | −1.3 | 4.6 | 3.4 | 2.9 | 1297.1 | −2.6 | −3.3 | 1214.9 | −0.8 | −0.2 |
| $T_{1u}$ | 1428.8 | −0.3 | −0.7 | 6 | 5.3 | 3.9 | 1549.5 | −2.7 | −3.5 | 1460.1 | −2.2 | −1.8 |

frequencies leads to a remarkable closeness to the experiment, within 3.6 $cm^{-1}$ average deviation for all observable vibrations.[23] The DFT relative frequencies of the encapsulated systems are well reproduced for $H_g$ and $T_{1u}$ cases. However, it is important to note that DFT fails in the account of the sign for the radial $A_g$ shift. As discussed later, we accorded a special attention to the totally symmetric vibrations. In this light it is important to understand the DFT situation. For $Ar@C_{60}$ and $Kr@C_{60}$ both $A_g$ DFT-computed shifts are negative, instead of the remarked up and down experimental pattern. The reported results are those of B3LYP/6-31G*, but we checked and emphasized that the problem is quite general. For the sake of conciseness we will not present such details, just pointing that using other functionals (*e.g.* with Slater[24] or Becke[25] exchange functionals, coupled with VWN[26] for correlation part) and basis sets (richer Pople[27] basis sets or DGDZVP[28]) one finds the same trend.

Considering the good absolute values of the $A_g$ frequencies, but the wrong shifts, it results that DFT performs well for the $C_{60}$ cage itself (in the regime of firm covalent bonds) while it seems inappropriate for the range of van der Waals effects, responsible for the differences. The failure can be assigned to the problems in the long range behavior of the DFT functionals[29] certain non-standard schemes to amend this drawback being devised.[30] Without entering the area of DFT assessments, we point out that the endohedral fullerenes offer rather particular cases for the study of such DFT drawbacks notably the almost spherical symmetry since, generally, other van der Waals contacts show lower symmetries and the cumulating 60 interatomic potentials, which offer a good resolution of the effect related to the functional extrapolation at the van der Waals radius.

The DFT slight irregularities prompted us to further employ the MP2 calculations. A full approach to the vibration spectrum is prohibitive at the MP2 level, but, as shown later, a correspondingly designed potential energy scan as a function of the $A_g$ nuclear coordinates afforded us these vibration numbers, altogether with an assessment of the MP2 performance. The MP2 frequencies results will be discussed in a next section, noting here that the method retrieves the correct tendency of the $A_g$ mode of radial type, which depends directly on the van der Waals potential.

### *Ab initio* optimized geometries

Concerning the $C_{60}$ geometry, the DFT and MP2 methods perform equally well, given the certain error affecting the known experimental data.[31] Subtle differences appear however between methods in the question of radial changes at encapsulation. In the $Ar@C_{60}$ and $Kr@C_{60}$ molecules, the B3LYP points toward a slightly enlarged cage, while MP2 optimizes a slightly shrunk one. The shrinkage would be a proof of the fact that the encapsulated atom benefits from a bonding stabilization (though small). The question of bonded *vs.* repulsive regime was initially a matter of dispute,[32] but the revisited conclusions[33] pointed towards a stabilization effect *e.g.* with MP2, taken however at a B3LYP geometry, of about −2.4 kcal $mol^{-1}$.[31]

It is worth to examine also the ratio of the bond lengths $l_1/l_2$ ($l_1$ and $l_2$ correspond to double and single bonds, see eqn (1a) and (1b)) as a function of molecular system and computation method. A related geometry parameter is $\tau$, designed to be zero at equal bond lengths. The parameters are summarized in Table 2. Taking the bond length ratio as a criterion for aromaticity, one may see that the series HF, DFT, MP2 yields a progressive increase of the aromatic character (the shift of $l_1/l_2$ toward unity and the decrease of $\tau$). Since the resonance is ultimately a correlation effect, one may assign the tendency to the amount of correlation accounted in the given methods, crediting then the MP2 with the most realistic resolution of the aromatic nature of the systems. In the series $C_{60}$, $Ar@C_{60}$, $Kr@C_{60}$ the MP2 calculations suggest a small but monotonous increase of aromaticity. Comparatively, the HF performs non-monotonously and DFT is almost inert in discriminating an $l_1/l_2$ variation at encapsulation.

**Table 2** Experimental and computed geometry parameters of $C_{60}$, $Ar@C_{60}$ and $Kr@C_{60}$

| | | $l_1$/Å | $l_2$/Å | $l_1/l_2$ | $\tau$ | $R$/Å | $\Delta R^a$/Å |
|---|---|---|---|---|---|---|---|
| Exp. | $C_{60}$ (NMR)[31a] | 1.400(15) | 1.450(15) | 0.966(20) | 0.0116(69) | 3.55(4) | |
| | $C_{60}$ (el-diffraction)[31b] | 1.401(10) | 1.458(6) | 0.961(11) | 0.0132(37) | 3.56(2) | |
| HF/6-31G* | $C_{60}$ | 1.373199 | 1.448622 | 0.947935 | 0.017662 | 3.522426 | — |
| | $Ar@C_{60}$ | 1.373545 | 1.449458 | 0.947626 | 0.017768 | 3.524061 | 0.001636 |
| | $Kr@C_{60}$ | 1.373706 | 1.44953 | 0.947691 | 0.017746 | 3.524318 | 0.001892 |
| B3LYP/6-31G* | $C_{60}$ | 1.395201 | 1.453460 | 0.959917 | 0.013542 | 3.549712 | — |
| | $Ar@C_{60}$ | 1.395729 | 1.453966 | 0.959946 | 0.013532 | 3.550984 | 0.001272 |
| | $Kr@C_{60}$ | 1.395759 | 1.453920 | 0.959997 | 0.013514 | 3.550939 | 0.001226 |
| MP2/6-31G* | $C_{60}$ | 1.407155 | 1.446900 | 0.972531 | 0.009241 | 3.549967 | — |
| | $Ar@C_{60}$ | 1.407307 | 1.446769 | 0.972724 | 0.009175 | 3.549893 | −0.00007 |
| | $Kr@C_{60}$ | 1.407251 | 1.446209 | 0.973062 | 0.009061 | 3.548955 | −0.00101 |

[a] Difference between the radius of $A@C_{60}$ and $C_{60}$.

**Analytical modeling. The $A_g$ modes as key of the vibration shift pattern**

The vibration frequencies in the encapsulated systems, as compared to the $C_{60}$, show that the lowest frequencies, related with the radial character ($1 \times A_g$, $3 \times H_g$ and $2 \times T_{1u}$), undergo a positive shift while the higher vibrations, with tangential character ($1 \times A_g$, $5 \times H_g$ and $2 \times T_{1u}$), show negative shifts.

A clue of quantitative description is found considering the $A_g$ problem as the causal seed of the vibration pattern. The other coordinates can be conceptually thought as resulted from modulation of $A_g$ ones with corresponding angular factors. The two $A_g$ vibrations act as barycenters for correspondingly grouped other symmetry modes. The $A_g$ modes can be fully modeled analytically with the help of two parameters, $R$ the radius of the sphere and $\tau$ that accounts for the differentiation in the bond lengths. The relationship of the above parameters with the two bond length types is as follows:

$$l_1 = l_{C=C} = 2R(1-2\tau)\Big/\sqrt{9\gamma^2 + (1-2\tau)^2} \qquad (1a)$$

$$l_2 = l_{C-C} = 2R(1+\tau)\Big/\sqrt{9\gamma^2 + (1-2\tau)^2}. \qquad (1b)$$

At hypothetically equal C–C and C=C bond lengths the $\tau$ value is zero. The collective coordinates (orthogonal, not normalized) of radial and tangential components are, respectively:

$$q(A_g)^i_R = \frac{d}{dR}\{x_i, y_i, z_i\} \qquad (2a)$$

$$q(A_g)^i_\tau = \frac{d}{d\tau}\{x_i, y_i, z_i\} \qquad (2b)$$

The first correspond to a uniform radial rescaling and the second to the alteration of the C=C *vs.* C–C bond length ratio. Taking the derivatives of molecular energy:

$$V_{RR} = \frac{\partial^2 E}{\partial R^2}, \quad V_{\tau\tau} = \frac{\partial^2 E}{\partial \tau^2}, \quad V_{R\tau} = \frac{\partial^2 E}{\partial R \partial \tau}, \qquad (3)$$

the equation of the $A_g$ modes results as follows:

$$\begin{vmatrix} V_{RR} - M_R \cdot \lambda & V_{R\tau} \\ V_{R\tau} & V_{\tau\tau} - M_\tau R^2 \cdot \lambda \end{vmatrix} = 0, \qquad (4)$$

where the effective masses of the radial and tangential modes are, respectively:

$$M_R = 60 m_C \qquad (5a)$$

$$M_\tau = \frac{17\,280(33 + 14\sqrt{5} - 2(3+\sqrt{5})\tau + 2(3+\sqrt{5})\tau^2)}{(29 + 9\sqrt{5} - 8\tau + 8\tau^2)^3} m_C, \qquad (5b)$$

with $m_C$ the mass of one carbon atom. Taking the parameters and the eigenvalues $\lambda$ in atomic units (Hartree for energy and Bohr for length), the conversion to frequencies in $cm^{-1}$ reads as follows $\nu = 5140.4874\sqrt{\lambda}$.

For the HF and DFT methods, where the frequency calculation is accessible, the parameters can be projected out from the full Hessian. In the case of MP2, where the full frequency calculation was not possible, we used a grid with $\Delta\tau = (-0.005, 0.0, +0.005)$ and $\Delta R = (-0.02, 0.0, +0.02$ Å) steps around the optimized equilibrium points described by the parameters of corresponding entries in Table 2. We checked the reliability of the procedure comparing the numerical Hessian, approached in the described model, and the one available from analytical projection, in the case of the HF method, obtaining good coincidence for the results. The relevant MP2 parameters are presented in Table 3. The Hessian analysis shows that the positive *vs.* negative shifts in the lower and higher vibrations are already contained in the diagonal force constants of radial *vs.* tangential pure modes.

The differences in the $V_{RR}$ of $A@C_{60}$ with respect to the empty $C_{60}$ can be assigned to an increment resulted from the placement of $A\cdots C$ distance within the zone with a positive curvature, around the minimum point of the intermolecular potential. Assuming a Lennard-Jones potential, we were able to estimate the parameters of the van der Waals interaction, as detailed later.

**Table 3** The MP2 data for the model of $A_g$ modes. Frequencies ($\upsilon$, in $cm^{-1}$) and force constants ($V_{RR}$, in Hartree $Bohr^{-2}$, $V_{\tau\tau}$, in Hartree, $V_{R\tau}$, in Hartree $Bohr^{-1}$) for $C_{60}$, $ArC_{60}$ and $KrC_{60}$ respectively. Note that $\tau$ is a dimensionless parameter

| | $\upsilon_1(A_g)$ | $\upsilon_2(A_g)$ | $V_{RR}$ | $V_{\tau\tau}$ | $V_{R\tau}$ |
|---|---|---|---|---|---|
| $C_{60}$ | 496.55 | 1532.28 | 6.7192 | 451.1018 | 0.6541 |
| $Ar@C_{60}$ | 496.95 | 1532.07 | 6.7301 | 450.9492 | 0.6723 |
| $Kr@C_{60}$ | 497.96 | 1533.61 | 6.7576 | 451.6019 | 0.7125 |

The negative shift in tangential modes can be tentatively explained considering that a source of negative contributions to the force constants is the so-called vibronic component of given force constants.[34] The vibronic part is a second-order effect, due to the coupling between ground and excited states, along a given normal coordinate. Our suggestion is that the A@$C_{60}$ system has more configuration interaction channels than the $C_{60}$, having therefore a supplement in the negative vibronic components. This is because the intruded atom offers a set of empty diffuse atomic orbitals which can interact with the cage. The supplementary vibronic components can be speculated as the cause of lowering the absolute value of tangential force constants, in the absence of other contributions to the non-vibronic counterparts. The non-vibronic effects are coming directly from potentials, such as the van der Waals host–guest interaction in the case of radial modes.

An alternate description of the tangential mode shift can be speculated in terms of aromaticity. Since the encapsulation causes an incremental trend toward the bond equalisation, one may say that filled fullerenes are infinitesimally more aromatic than the $C_{60}$. However, since the bond-length shift is small and the aromaticity in fullerene is a rather controversial issue,[35,36] various proofs affirming[37] or denying[38] this feature, we advance this suggestion with caution.

According to vibration frequency (near 1500 $cm^{-1}$) and the visual inspection of the computed normal coordinate, the tangential $A_g$ movements can be described as dominantly along the C=C bonds. The incremental delocalization, accompanying the small surge of aromaticity, weakens this force constant.

### Extracting van der Waals interaction parameters

We propose here a model affording the estimation of host–guest interaction parameters based on force constant and geometry displacements in endohedrals. Thus, assigning for the fullerene itself a harmonic potential equated in the pure radial term, while the van der Waals effects are taken under the Lennard-Jones parameterization, the total energy of the endohedral system is:

$$E(R) = \frac{1}{2} V^0_{RR}(R - R_0)^2 - A\left(\frac{1}{R^6} - \frac{1}{2}\frac{\rho^6}{R^{12}}\right), \qquad (6)$$

where $V^0_{RR}$ and $R_0$ are the force constant and equilibrium radius of the empty fullerene and $\rho$ the equilibrium point of the van der Waals potential energy curve. Considering that the endohedral fullerene shows a new equilibrium structure, with the $R_1$ radius and shifted force constant $V^1_{RR}$, we can equate the new minimum of energy in the following form:

$$\left(\frac{d}{dR}E(R)\right)_{R=R_1} = V^0_{RR}(R_1 - R_0) + A\left(\frac{6}{R_1^7} - \frac{6\rho^6}{R_1^{13}}\right) = 0, \qquad (7)$$

and the new force constants as:

$$\left(\frac{d^2}{dR^2}E(R)\right)_{R=R_1} = V^1_{RR} = V^0_{RR} - A\left(\frac{42}{R_1^8} - \frac{78\rho^6}{R_1^{14}}\right). \qquad (8)$$

The knowledge of new molecular data $V^1_{RR}$ and $R_1$ *vs.* those of the unperturbed system, $V^0_{RR}$ and $R_0$, enables the determination of

**Table 4** Lennard-Jones parameters ($\rho$, in Å, and $A$, in atomic unit) related to one $A\cdots C$ diatomic potential in A@$C_{60}$ and the correspondingly estimated van der Waals total host–guest interaction energy ($E_{vdW}$ in kcal $mol^{-1}$): (a) using MP2 geometries and MP2 $A_g$ frequencies; (b) using MP2 geometries and the experimental $A_g$ frequencies

| | | $\rho$ | $A$ | $E_{vdW}$ |
|---|---|---|---|---|
| Ar@$C_{60}$ | $a_1$ | 3.510 | 24.162 | −5.317 |
| Kr@$C_{60}$ | $a_2$ | 3.432 | 119.955 | −29.305 |
| Ar@$C_{60}$ | $b_1$ | 3.517 | 29.435 | −6.411 |
| Kr@$C_{60}$ | $b_2$ | 3.344 | 73.880 | −19.856 |

$A$ and $\rho$ parameters of the Lennard-Jones potential. Table 4 shows the values together with the energy at the actual position of the $A\cdots C$ radius ($E_{vdW}$) and Fig. 2 displays the $A\cdots C$ potentials.

In the case of A@$C_{60}$ the brute force calculation of the radial dependence of the van der Waals energy faces a particular problem. Namely, the $R$ variation enforces the stretch coordinate of the 90 carbon–carbon bonds in the $C_{60}$ skeleton that supersedes by orders of magnitude the contribution of the 60 $A\cdots C$ van der Waals contacts. The regular intermolecular interaction energy estimations, involving separate molecular entities usually do not meet such a situation that complicates the usual numerical sensitivity of van der Waals effects taken as molecular energy difference.

The outlined model enables a rather inedited circumventing of the noted accuracy problem. Working with vibration frequency data, as a source of interaction potentials, we are using a more appropriate energy scale ($\sim 10^{-3}$ Hartree) that is practically in the same range with the van der Waals amount. This procedure is lesser prone to numerical errors than the usual route, working with differences in the *ab initio* molecular energies whose range is $\sim 10^3$ Hartree. Besides, in the new phenomenological frame there is no need to consider any basis set superposition correction (BSSE) since the $R_1$ and $V^1_{RR}$

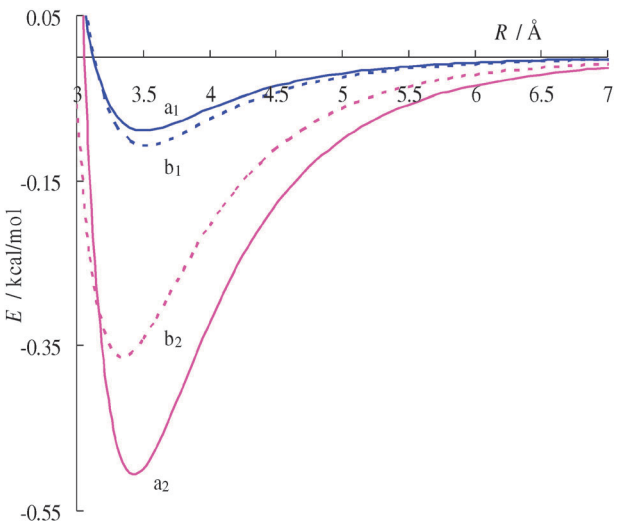


**Fig. 2** The estimated Lennard-Jones potentials related to one $A\cdots C$ diatomic pair in the A@$C_{60}$ systems. The curves $a_1$ and $a_2$ correspond to Ar@$C_{60}$ and Kr@$C_{60}$, respectively, obtained by the outlined model, using the MP2 frequencies and geometry parameters. The curves $b_1$ and $b_2$ are for Ar@$C_{60}$ and Kr@$C_{60}$, respectively, using the experimental frequencies and the MP2 geometry parameters.

directly rely on the full computation of the $A@C_{60}$ system while $R_0$ and $V^0_{RR}$ refer to the empty $C_{60}$, without assuming any other computational or conceptual complications.

The method works better in the cases when analytical gradients and Hessians are available. In the case of numerical Hessians certain errors may still persist. However, since numerical Hessians are obtained from calculations pertaining to the same setting, one may advocate smaller incorporated inaccuracies than in the case of calculations made in the different basis set balances, like the usual BSSE approach.

Probably the relative differences between $Ar@C_{60}$ and $Kr@C_{60}$ Lennard-Jones potentials are overestimated by some unbalanced effects in the frozen core part of the two systems, but the range of the data as well as the fact that the minimum of the van der Waals potential is slightly smaller than the $C_{60}$ radius are consistent results. The outlined model would allow in principle to estimate the interaction energy from experimental data, if precisely enough geometry data ($R_0$ and $R_1$) were experimentally available. However, as noted previously the experimental error in the data about the $C_{60}$ radius and $Kr@C_{60}$ one[9] is probably higher than the expected small net differences. Compromise estimation is possible using the MP2 computed geometry and the experimental frequencies. The Lennard-Jones curves estimated in this way (entries b in Table 4 and dashed line in Fig. 2) are probably closer to reality than those exclusively based on the MP2 data (entries a).

The absolute interaction parameters seem a rather delicate problem. Experimental data for the Ar···C interaction differ substantially to each other, about twice in the stabilization energy. Converted to our convention of Lennard-Jones potential, the different literature data read as the following ($\rho$, $A$) couples: (3.87, 114.95)[39] and (3.73, 55.74).[40] Applied at the approximate radius of the $C_{60}$ these correspond to the $-7.8$ kcal mol$^{-1}$ and $-7.5$ kcal mol$^{-1}$, in the circumstances of a substantially larger van der Waals radius, $\rho \approx 3.8$, as compared to the $C_{60}$ one, $R \approx 3.5$. At the same time, a direct estimation from MP2 formation energy reported $-2.4$ kcal mol$^{-1}$. Our parameterization yields an intermediate result, $-5.3$ kcal mol$^{-1}$, which seems reasonable.

### The other vibration modes

Without a full quantitative modeling, we can sketch the principle of treating the other modes in terms of spherical harmonics decomposition. As extrapolation, the shift pattern in $H_g$ and $T_{1u}$ will be understood as having the same causal roots, as a function of radial *vs.* tangential movements, similarly to the $A_g$ simpler case.

The radial components can be ascribed as the modulation of the radial $A_g$ reference with symmetry adapted spherical harmonics. The tangential modes can be treated as spherical harmonic vectors, behaving as fluxes on the sphere surface. As an example of the results obtained by this formalism, Fig. 3 shows the radial and the tangential character for the lowest $H_g$ vibration. This vibration presents about 73% radial character, the rest has a tangential component. The description of this treatment is given in the ESI.† As corollary of actual discussion, we suggest promising further advances in conceiving a new

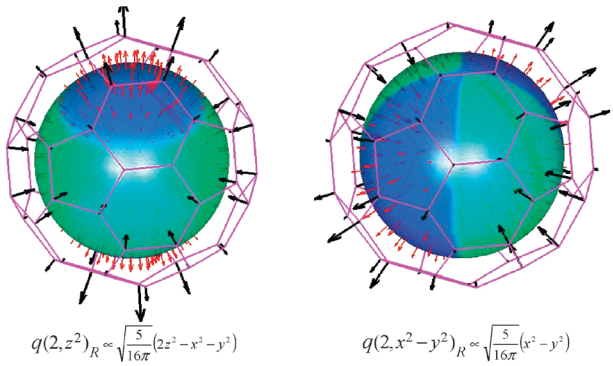


**Fig. 3** Selected members with $l = 2$ parentage for radial (spherical harmonics, $Y_{20} \propto z^2$ (left) and $Y_{22}{}^c \propto x^2 - y^2$ (right)) components in the lowest $H_g$ vibration. The colors on the inner sphere represent the sign (dark gray—positive, light gray—negative) of the selected spherical harmonics component. The length of arrows on the sphere is proportional to the magnitude of the $Y$ or $V$ functions. Their orientation depends on the $Y$ sign and nodes. The radial or tangential displacement of the cluster atoms is proportional to the $Y$ or $V$ functions, respectively, at the atom polar coordinates.

type of force field explicitly based on the radial *vs.* tangential dichotomy (instead of the regular neighbour bond parameters expansions).[41] Here we confined ourselves to a quantitative modeling of $A_g$ modes, the semiquantitative extrapolation on the $H_g$ ones, pointing in addition that the $T_{1u}$ case follows a similar qualitative principle.

## Conclusion

We measured the vibrational properties of pure $Ar@C_{60}$ and $Kr@C_{60}$. The intramolecular vibrational modes of $Ar@C_{60}$ and $Kr@C_{60}$ were systematically shifted compared to those of pristine $C_{60}$. The encapsulated noble gas atom causes a blue shift of the lower frequency features, and a red shift of higher frequency modes. We can understand these trends in terms of the interaction between the noble gas atom and the carbon cage. The $A\cdots C$ distance in $A@C_{60}$ ($A$ = Ar, Kr) is in the region of attractive, positive curvature in the Lennard-Jones potential curve, and thus underlies the observed blue shift of vibrational modes in $A@C_{60}$ with substantial radial character. The red shift of the tangential features in $A@C_{60}$ is related to aromaticity effects on the $C_{60}$ surface. Theoretical modelling explains very well the observed shifts in the frequencies.

## Acknowledgements

FC acknowledges CNCSIS-UEFISCSU support (Grant-PCE-174/2007). The authors would like to thank the staff of the Center for Computational Materials Science at the Institute for Materials Research in Sendai for computational assistance.

## Notes and references

1 J. R. Heath, S. C. O'Brien, Q. Zhang, Y. Liu, R. F. Curl, H. W. Kroto, F. K. Tittel and R. E. Smalley, *J. Am. Chem. Soc.*, 1985, **107**, 7779; T. Weiske, D. K. Böhme, J. Hrusák, W. Krätschmer and H. Schwarz, *Angew. Chem., Int. Ed. Engl.*,

 

1991, **30**, 884; T. A. Murphy, T. Pawlik, A. Weidinger, M. Höhne, R. Alcala and J.-M. Spaeth, *Phys. Rev. Lett.*, 1996, **77**, 1075–1078; J. A. Larsson, J. C. Greer, W. Harneit and A. Weidinger, *J. Chem. Phys.*, 2002, **116**, 7849–7854.
2 M. Murata, Y. Murata and K. Komatsu, *J. Am. Chem. Soc.*, 2006, **128**, 8024–8033; T. Suetsuna, N. Dragoe, W. Harneit, A. Weidinger, H. Shimotani, H. Takagi and K. Kitazawa, *Chem.–Eur. J.*, 2002, **8**, 5079–5083.
3 T. Weiske, D. K. Böhme, J. Hrusák, W. Krätschmer and H. Schwarz, *Angew. Chem., Int. Ed. Engl.*, 1991, **30**, 884–886; M. Saunders, H. A. Jiménez-Vázquez, R. J. Cross and R. J. Poreda, *Science*, 1993, **259**, 1428.
4 M. E. Madjet, H. S. Chakraborty and S. T. Manson, *Phys. Rev. Lett.*, 2007, **99**, 243003.
5 (*a*) D. S. Bethune, R. D. Johnson, J. R. Salem, M. S. Devries and C. S. Yannoni, *Nature*, 1993, **366**, 123–128; (*b*) Y. Takabayashi, Y. Kubozono, K. Hiraoka, T. Inoue, K. Mimura, H. Maeda and S. Kashino, *Chem. Lett.*, 1997, 1019–1020; (*c*) H. Shinohara, *Rep. Prog. Phys.*, 2000, **63**, 843–892; (*d*) Y. Kubozono, T. Inoue, Y. Takabayashi, S. Fujiki, S. Kashino, T. Akasaka, T. Wakahara, M. Inakuma, H. Kato, T. Sugai, H. Shinohara and S. Emura, *J. Synchrotron Radiat.*, 2001, **8**, 551–553; (*e*) L. Dunsch, P. Georgi, M. Krause and C. R. Wang, *Synth. Met.*, 2003, **135**, 761–762; (*f*) C. N. Ramachandran, D. Roy and N. Sathyamurthy, *Chem. Phys. Lett.*, 2008, **461**, 87–92; (*g*) M. N. Chaur, R. Valencia, A. Rodriguez-Fortea, J. M. Poblet and L. Echegoyen, *Angew. Chem., Int. Ed.*, 2009, **48**, 1425–1428; (*h*) A. Hirsh, *Nat. Mater.*, 2010, **9**, 868–871; (*i*) S. Aoyagi, E. Nishibori, H. Sawa, K. Sugimoto, M. Takata, Y. Miyata, R. Kitaura, H. Shinohara, H. Okada, T. Sakai, Y. Ono, K. Kawachi, K. Yokoo, S. Ono, K. Omote, Y. Kasama, S. Ishikawa, T. Komuro and H. Tobita, *Nat. Chem.*, 2010, **2**, 678–683.
6 M. Saunders, H. A. Jiménez-Vázquez, R. J. Cross, S. Mroczkowski, D. I. Freedberg and F. A. L. Anet, *Nature*, 1994, **367**, 256–258.
7 K. Yamamoto, M. Saunders, A. Khong, R. J. Cross, M. Grayson, M. L. Gross, A. F. Benedetto and R. B. Welsman, *J. Am. Chem. Soc.*, 1999, **121**, 1591; T. Suetsuna, N. Dragoe, H. Shimotani, A. Takeda, S. Ito, R. J. Cross, M. Saunders, H. Takagi and K. Kitazawa, *Fullerenes, Nanotubes, Carbon Nanostruct.*, 2002, **10**, 15.
8 M. S. Syamala, R. J. Cross and M. Saunders, *J. Am. Chem. Soc.*, 2002, **124**, 6216.
9 S. Ito, A. Takeda, T. Miyazaki, Y. Yokoyama, M. Saunders, R. J. Cross, H. Takagi, P. Berthet and N. Dragoe, *J. Phys. Chem. B*, 2004, **108**, 3191.
10 H. M. Lee, M. M. Olmstead, T. Suetsuna, H. Shimotani, N. Dragoe, R. J. Cross, K. Kitazawa and A. L. Balch, *Chem. Commun.*, 2002, 1352.
11 M. Morscher, A. Seitsonen, S. Ito, H. Takagi, N. Dragoe and T. Greber, *Phys. Rev. A: At., Mol., Opt. Phys.*, 2010, **82**, 051201.
12 M.-S. Son and Y. K. Sung, *Chem. Phys. Lett.*, 1995, **245**, 113–118; Z.-Y. Wang, K.-H. Su, X.-P. Yao, Y.-L. Li and F. Wang, *Mater. Chem. Phys.*, 2010, **119**, 406–417; V. V. Albert, J. R. Sabin and F. E. Harris, *Int. J. Quantum Chem.*, 2007, **107**, 3061–3066; Z. Wang, D. Li, K. Su, H. Fan, Y.-L. Li and Z. Wen, *Chem. Phys.*, 2007, **331**, 309–320.
13 R. J. Cross, A. Khong and M. Saunders, *J. Org. Chem.*, 2003, **68**, 8281.
14 S. Brown, J. Cao, J. L. Musfeldt, N. Dragoe, F. Cimpoesu, S. Ito, H. Takagi and R. J. Cross, *Phys. Rev. B: Condens. Matter Mater. Phys.*, 2006, **73**, 125446.
15 (*a*) T. Sternfeld, M. Saunders, R. J. Cross and M. Rabinovitz, *Angew. Chem., Int. Ed.*, 2003, **42**, 3136; (*b*) M. Bühl, *Chem.–Eur. J.*, 1998, **4**, 734–739; (*c*) M. Saunders, R. J. Cross, H. A. Jiménez-Vázquez, R. Shimshi and A. Khong, *Science*, 1996, **271**, 1693–1697.
16 S. J. Duclos, R. C. Haddon, S. Glarum, A. F. Hebard and K. B. Lyons, *Science*, 1991, **254**, 1625.
17 A. Takeda, Y. Yokoyama, S. Ito, T. Miyazaki, H. Shimotani, K. Yakigaya, T. Kakiuchi, H. Sawa, H. Takagi, K. Kitazawa and N. Dragoe, *Chem. Commun.*, 2006, 912–914.
18 J. L. Dunn and C. A. Bates, *Phys. Rev. B: Condens. Matter*, 1995, **52**, 5996; R. C. Haddon, L. E. Brus and K. Raghavachari, *Chem. Phys. Lett.*, 1986, **125**, 459; O. Gunnarsson, *Rev. Mod. Phys.*, 1997, **69**, 575; A. Ceulemans, L. F. Chibotaru and F. Cimpoesu, *Phys. Rev. Lett.*, 1997, **78**, 3275–3728.
19 Y. Yakigaya, A. Takeda, Y. Yokoyama, S. Ito, T. Miyazaki, T. Suetsuna, H. Shimotani, T. Kakiuchi, H. Sawa, H. Takagi, K. Kitazawa and N. Dragoe, *New J. Chem.*, 2007, **31**, 973–979.
20 (*a*) S. Ito, A. Takeda, T. Miyazaki, Y. Yokoyama, M. Saunders, R. J. Cross, H. Takagi, P. Berthet and N. Dragoe, *J. Phys. Chem. B*, 2004, **108**, 3191–3195; (*b*) T. Suetsuna, N. Dragoe, W. Harneit, A. Weidinger, H. Shimotani, S. Ito, H. Takagi and K. Kitazawa, *Chem.–Eur. J.*, 2002, **8**, 5079–5083.
21 M. J. Frisch, G. W. Trucks, H. B. Schlegel, G. E. Scuseria, M. A. Robb, J. R. Cheeseman, V. G. Zakrzewski, J. A. Montgomery, R. E. Stratmann, J. C. Burant, S. Dapprich, J. M. Millam, A. D. Daniels, K. N. Kudin, M. C. Strain, O. Farkas, J. Tomasi, V. Barone, M. Cossi, R. Cammi, B. Mennucci, C. Pomelli, C. Adamo, S. Clifford, J. Ochterski, G. A. Petersson, P. Y. Ayala, Q. Cui, K. Morokuma, D. K. Malick, A. D. Rabuck, K. Raghavachari, J. B. Foresman, J. Cioslowski, J. V. Ortiz, B. B. Stefanov, G. Liu, A. Liashenko, P. Piskorz, I. Komaromi, R. Gomperts, R. L. Martin, D. J. Fox, T. Keith, M. A. Al-Laham, C. Y. Peng, A. Nanayakkara, C. Gonzalez, M. Challacombe, P. M. W. Gill, B. G. Johnson, W. Chen, M. W. Wong, J. L. Andres, M. Head-Gordon, E. S. Replogle and J. A. Pople, Gaussian, Inc., Pittsburgh PA, 1998.
22 H. W. Kroto, A. W. Allaf and S. P. Balm, *Chem. Rev.*, 1991, **91**, 1213–1235.
23 V. Schettino, M. Pagliai, L. Ciabini and G. Cardini, *J. Phys. Chem. A*, 2001, **105**, 11192.
24 J. C. Slater, *Quantum Theory of Molecular and Solids*, *The Self-Consistent Field for Molecular and Solids*, McGraw-Hill, New York, 1974, vol. 4.
25 A. D. Becke, *J. Chem. Phys.*, 1996, **104**, 1040.
26 S. H. Vosko, L. Wilk and M. Nusair, *Can. J. Phys.*, 1980, **58**, 1200.
27 R. Krishnan, J. S. Binkley, R. Seeger and J. A. Pople, *J. Chem. Phys.*, 1980, **72**, 650; A. D. McLean and G. S. Chandler, *J. Chem. Phys.*, 1980, **72**, 5639; L. A. Curtiss, M. P. McGrath, J.-P. Blaudeau, N. E. Davis, R. C. Binning Jr. and L. Radom, *J. Chem. Phys.*, 1995, **103**, 6104.
28 C. Sosa, J. Andzelm, B. C. Elkin, E. Wimmer, K. D. Dobbs and D. A. Dixon, *J. Phys. Chem.*, 1992, **96**, 6630.
29 T. Leininger, H. Stoll, H.-J. Werner and A. Savin, *Chem. Phys. Lett.*, 1997, **275**, 151; W. Kohn, Y. Meir and D. E. Makarov, *Phys. Rev. Lett.*, 1998, **80**, 4153; T. V. Mourik and R. J. Gdanitz, *J. Chem. Phys.*, 2002, **116**, 9620.
30 Y. Andersson, D. C. Langreth and B. I. Lundqvist, *Phys. Rev. Lett.*, 1996, **76**, 102; M. Kamiya, T. Tsuneda and K. Hirao, *J. Chem. Phys.*, 2002, **117**, 6010; T. Sato, T. Tsuneda and K. Hirao, *Mol. Phys.*, 2005, **103**, 1151.
31 (*a*) K. Hedberg, L. Hedberg, D. S. Bethune, C. A. Brown, H. C. Dorn, R. D. Johnson and M. Devries, *Science*, 1991, **254**, 410–412; (*b*) C. S. Yannoni, P. P. Bernier, D. S. Bethune, G. Meijer and J. R. Salem, *J. Am. Chem. Soc.*, 1991, **113**, 3190–3192.
32 R. B. Darzynkiewicz and G. E. Scuseria, *J. Phys. Chem. A*, 1998, **102**, 7143; M. Buehl, S. Patchkovskii and W. Thiel, *Chem. Phys. Lett.*, 1997, **275**, 14.
33 J. M. Hawkins, A. Meyer, T. A. Lewis, S. Loren and F. J. Hollander, *Science*, 1991, **252**, 312.
34 I. B. Bersuker, *Chem. Rev.*, 2001, **101**, 1067–1114.
35 R. C. Haddon, *J. Am. Chem. Soc.*, 1997, **119**, 1797–1798.
36 J. Poater, X. Fradera, M. Duran and M. Solà, *Chem.–Eur. J.*, 2003, **9**, 1113–1122.
37 P. Fowler, *Nature*, 1991, **350**, 20; R. C. Haddon, *Nature*, 1995, **378**, 249.
38 A. Hirsch, *Angew. Chem., Int. Ed. Engl.*, 1993, **32**, 1138; A. Hirsch, *Top. Curr. Chem.*, 1999, **199**, 1.
39 S. Iglesias-Groth, J. Breton and C. Girardet, *Chem. Phys.*, 1998, **237**, 285–293.
40 M.-S. Son and Y. K. Sung, *Chem. Phys. Lett.*, 1995, **245**, 113–118.
41 Z. C. Wu, D. A. Jelski and T. F. George, *Chem. Phys. Lett.*, 1987, **137**, 291; R. A. Jishi, R. M. Mirie and M. S. Dresselhaus, *Phys. Rev. B: Condens. Matter*, 1992, **45**, 13685; A. Ceulemans, B. C. Titeca, L. F. Chibotaru, I. Vos and P. W. Fowler, *J. Phys. Chem. A*, 2001, **105**, 8284; I. D. Hands, J. L. Dunn and C. A. Bates, *J. Chem. Phys.*, 2004, **120**, 6912–6921.